

Ab initio study of the ferroelectric strain dependence and 180° domain walls in the barium metal fluorides BaMgF₄ and BaZnF₄

Maribel Núñez Valdez*

Materials Theory, ETH Zürich, Wolfgang-Pauli-Strasse 27, CH-8093 Zürich, Switzerland
Moscow Institute of Physics and Technology, Dolgoprudny, Moscow Region, Russia

Hendrik Th. Spanke and Nicola A. Spaldin

Materials Theory, ETH Zürich, Wolfgang-Pauli-Strasse 27, CH-8093 Zürich, Switzerland
(Dated: November 3, 2015)

We investigate the strain dependence of the ferroelectric polarization and the structure of the ferroelectric domain walls in the layered perovskite-related barium fluorides, BaMF₄ (M=Mg, Zn). The unusual “geometric ferroelectricity” in these materials is driven by the softening of a single polar phonon mode consisting of rotations of the MF₆ octahedra accompanied by polar displacements of the Ba cations, and in contrast to conventional ferroelectrics involves minimal electronic rehybridization. We therefore anticipate a different strain dependence of the polarization, and alternative domain wall structures compared with those found in conventional ferroelectric materials. Using first-principles calculations based on density functional theory (DFT) within the general gradient approximation (GGA), we calculate the variation of the crystal structure and the ferroelectric polarization under both compressive and tensile strain. We perform structural relaxations of neutral domain walls between oppositely oriented directions of the ferroelectric polarization and calculate their corresponding energies to determine which are most likely to form. We compare our results to literature values for conventional perovskite oxides to provide a source of comparison for understanding the ferroelectric properties of alternative non-oxide materials such as the barium fluorides.

I. INTRODUCTION

Ferroelectric and multiferroic oxides are widely studied because of their fundamental interest and for technological applications such as non-volatile random access memories¹, piezoelectric actuators and sensors², pyroelectric detectors³, and electro-optic and non-linear optical devices⁴. Indeed, it is often assumed that the presence of oxygen, which forms highly polarizable bonds with transition metal cations, is a requirement for good ferroelectric behavior. Recently, however, research on ferroelectric materials based on alternative chemistries without oxygen has received renewed interest. In particular, the class of barium metal fluorides, BaMF₄ (for a review see Ref. 5 and references therein), such as BaMgF₄⁶ could prove to be important because of the wide band gaps and associated transparency of fluorine-based compounds, which makes them attractive for advanced photonic and optoelectronic applications⁷.

The BaMF₄ barium metal fluorides form in a bilayered, perovskite-related base-centered orthorhombic structure (space group No. 36, *Cmc*2₁) as shown in Fig. 1. The divalent M cation can be a 3d transition metal ion (Mn, Fe, Co or Ni) or a non-magnetic divalent ion (Mg or Zn), and is octahedrally coordinated by fluorine anions. Two-layer slabs of corner-sharing MF₆ octahedra lie perpendicular to the crystallographic *b*-axis with Ba cations in planes between the slabs^{9,10}. The structure is polar, and ferroelectric switching using a pulsed-field technique has been demonstrated at room temperature for all members of the BaMF₄ family except for M = Mn and Fe^{5,10}. The high-temperature paraelectric reference phase has not been identified experimentally, because melting oc-

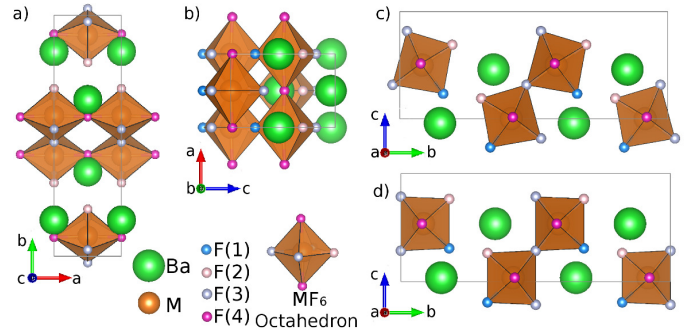


FIG. 1. (Color online) Structure of BaMgF₄. a-c) Ferroelectric *Cmc*2₁ phase in different orientations. The calculated lowest energy structure, which is similar to the experimental one, is shown. d) Hypothetical *Ccm* centrosymmetric reference phase. The ferroelectric and centrosymmetric structures of BaZnF₄ are qualitatively similar to those of BaMgF₄. The conventional primitive unit cell, which contains 24 atoms (four formula units), is indicated in gray. (All crystal visualizations in this paper were performed using VESTA⁸).

curs before the ferroelectric Curie temperature, T_C (estimated to be between 1100 and 1600 K by extrapolating the temperature-dependent dielectric constants¹¹) is reached. First-principles electronic structure calculations have shown, however, that the ferroelectric ground state can be reached from a prototypical centrosymmetric *Ccm* structure [Fig. 1 (d)] via a single polar phonon mode which consists of a rotation of the MF₆ octahedra accompanied by a displacement of the Ba²⁺ atoms along the *b* axis¹². The driving force for this so-called *geometric ferroelectricity* is the combination of size effects and

the layered geometric coordination of the crystal lattice, rather than the usual electronic rehybridization found in conventional ferroelectrics. As a result, the Born effective charges, which reflect the degree of rehybridization during a polar distortion, are close to the formal ionic charges in contrast to the anomalously large values characteristic of conventional ferroelectrics. The same mechanism is believed to occur in the layered, perovskite-related rare-earth titanates $\text{R}_2\text{Ti}_2\text{O}_7$ ^{13,14} and a related improper version occurs in the hexagonal rare-earth manganites^{15,16}.

We anticipate that this unconventional mechanism for the ferroelectric polarization in the BaMF_4 family might lead to quite different behavior in two properties that are particularly relevant for the incorporation of ferroelectrics into thin film devices. The first is the strain dependence of the ferroelectric polarization, which is particularly important when ferroelectrics are grown on substrates with mismatched lattice constants. The polarization-lattice coupling is substantial in many conventional oxide ferroelectrics¹⁷, and is believed to be driven by the large electronic rehybridizations reflected in the anomalous Born effective charges, therefore we expect smaller effects here. The second is the nature of the domain walls separating regions of opposite polarization. These have been studied extensively both theoretically and experimentally in conventional ferroelectric perovskite oxides because they have a profound influence on the material physical properties, in particular the ferroelectric hysteresis. The identity and structure of the lowest energy domain walls in conventional perovskite oxides are now well established (see for example Refs. [18–21]). In addition, the interaction of domain walls with point defects such as oxygen vacancies, and the resulting effects on the properties are topics of tremendous current interest²². With the unusual rotational mechanism for ferroelectricity in BaMF_4 , the domain walls might more closely resemble anti-phase boundaries, with different energetics and thicknesses from their conventional ferroelectric counterparts. To the best of our knowledge, however, calculations exploring the strain dependence of polarization and the structure and properties of the domain walls in BaMF_4 ferroelectrics have not been performed; this is the goal of this work.

The remainder of this paper is organized as follows: In section II we describe the technical details of our calculations. Section III, the main part of the article, contains our results for our two representative materials, BaMgF_4 and BaZnF_4 . Specifically, we present the structures of the low-energy neutral domain walls obtained using structural optimizations of atomic positions, and the dependence of the spontaneous polarization on the strain. In section IV we summarize our main findings and present our conclusions.

II. COMPUTATIONAL DETAILS

Our calculations were performed using the Vienna *Ab initio* Simulation Package (VASP)²³ within the projector-augmented plane wave (PAW)^{24,25} method of density functional theory (DFT)^{26,27}. We used the general-gradient approximation (GGA) in the prescription by Perdew, Burke and Ernzerhof (PBE)²⁸ for the exchange-correlation potential. We used the default PAW potentials with the valence electronic configurations $5s^25p^66s^2$ for Ba, $3d^{10}4s^2$ for Zn, $3s^2$ for Mg, and $2s^22p^5$ for F. A plane-wave cutoff energy of 500 eV and a Brillouin-zone k -point sampling of $6\times 4\times 6$ within the 24-atom unit cell were used. Convergence was assumed when the forces on each atom were smaller than 1 meV/Å and the total energy changes less than 10^{-8} eV. The electronic contributions to the spontaneous polarization (P_S), defined as the difference in polarization between the ferroelectric ground state structure ($Cmc2_1$) and the postulated high symmetry paraelectric phase ($Cmcm$), were calculated using the Berry phase approach^{29–31} by integrating over six homogeneously distributed k -point strings, parallel to the reciprocal crystallographic c -axis, each containing ten k -points.

TABLE I. Our calculated structural parameters [*] at zero temperature for the $Cmc2_1$ ferroelectric phases of BaMgF_4 and BaZnF_4 . Experimental data at 10 K from Ref. [32] for both materials, and DFT results from Ref. [33] for BaZnF_4 are shown for comparison. All atomic positions have Wyckoff symmetry $4a$.

Parameter	Mg		Zn		
	DFT [*]	EXP Ref. [32]	DFT [*]	EXP Ref. [33]	EXP Ref. [32]
a_0 (Å)	4.16	4.119	4.25	4.281	4.191
b_0 (Å)	14.83	14.463	14.88	14.700	14.513
c_0 (Å)	5.93	5.812	5.97	5.921	5.835
Ba x	0.5	0.5	0.5	0.5	0.5
y	0.350	0.351	0.351	0.3520	0.352
z	0.460	0.536	0.455	0.4575	0.537
M x	0.0	0.0	0.0	0.0	0.0
y	0.416	0.414	0.414	0.413	0.413
z	0.002	0.0	−0.002	0.0	0.0
F(1) x	0.0	0.0	0.0	0.0	0.0
y	0.338	0.306	0.335	0.333	0.303
z	0.734	0.803	0.726	0.727	0.800
F(2) x	0.0	0.0	0.0	0.0	0.0
y	0.304	0.334	0.302	0.301	0.330
z	0.191	0.261	0.193	0.198	0.262
F(3) x	0.0	0.0	0.0	0.0	0.0
y	0.527	0.473	0.531	0.531	0.471
z	0.817	0.692	0.831	0.830	0.673
F(4) x	0.5	0.5	0.5	0.5	0.5
y	0.422	0.422	0.423	0.423	0.422
z	0.015	−0.010	0.017	0.017	0.983

III. RESULTS

A. Structural, Electronic, and Ferroelectric Properties

We begin by calculating the lowest energy structures and lattice parameters for the bulk ferroelectric ($Cmc2_1$) phases of $BaMgF_4$ and $BaZnF_4$. Our 0 K results, shown in Table I, compare reasonably with experimental measurements at ~ 10 K extracted from synchrotron powder diffraction data³² and a previous DFT calculation for $BaZnF_4$ ³³. Our calculated atomic positions are in good agreement with the experimentally determined positions along the a and b directions, with larger deviations in the c direction. Likewise our a and c lattice parameters are close to the measured values, with a difference of $\sim 2.5\%$ for the b lattice parameter perpendicular to the layers, likely due to the GGA overestimating the weak bonding between the layers.

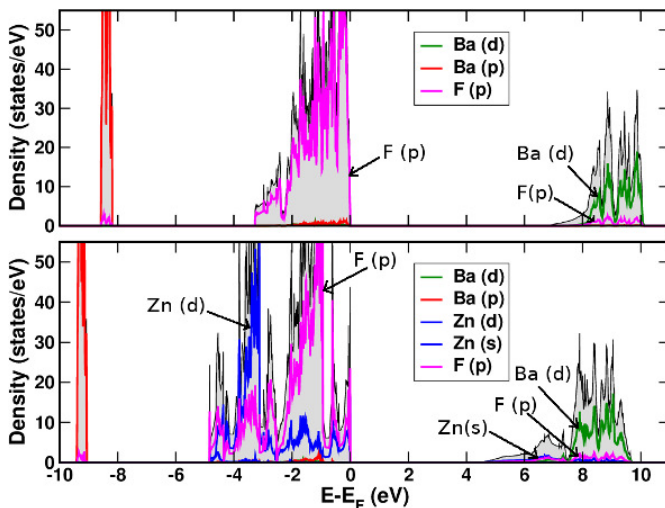


FIG. 2. (Color online) Total (black line and gray shaded) and partial (color) densities of states of bulk a) $BaMgF_4$ and b) $BaZnF_4$. $Ba\ p$ states are shown in red, $Ba\ d$ states in green, and $F\ p$ states in magenta. $Zn\ d$ and s states are in blue.

In Fig. 2 we show our calculated densities of states. We see that both compounds are strongly insulating with large DFT band gaps (6.9 and 4.5 eV for $BaMgF_4$ and $BaZnF_4$ respectively). The top of the valence bands is formed primarily from $F\ 2p$ states and the lower part of the conduction bands from $Ba\ 5d$ states, with negligible hybridization between them. A notable difference between the two materials is the presence of $Zn\ 3d$ states mixed with the $F\ 2p$ states at the bottom of the valence band in $BaZnF_4$, and $Zn\ 4s$ states at the bottom of the conduction band leading to the smaller gap in this case. $Mg\ s$ states are minimally present in the range shown.

Fig. 3 shows the dependence of the total energy per formula unit (f.u.) on the pattern of atomic displacements that transforms the paraelectric (PE) structure to the ground state ferroelectric (FE) structure for $BaMgF_4$.

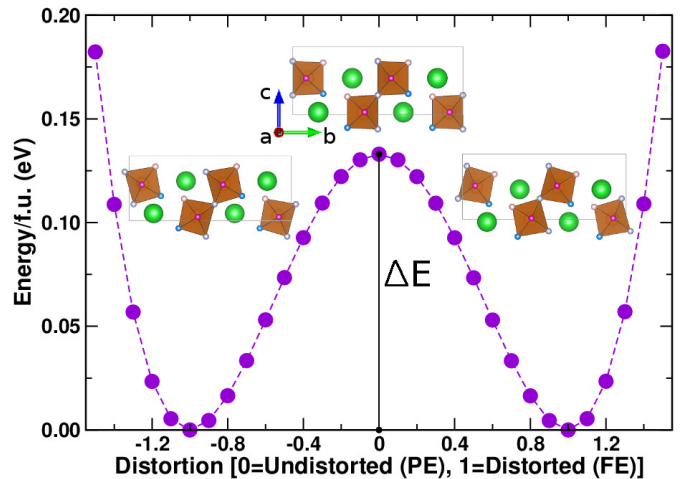


FIG. 3. (Color online) Energy per formula unit (f.u.) of $BaMgF_4$ as a function of the magnitude of the ferroelectric structural distortion. For $BaZnF_4$ the form of the double-well potential is qualitatively similar but the energy barrier, ΔE , is larger. The left and right insets show the MgF_6 octahedral rotation patterns in the two ferroic ground states compared to the unrotated PE phase (central inset).

We see the usual double-well potential characteristic of proper ferroelectrics with an energy barrier, ΔE , between the two equivalent ferroic ground states of 0.133 eV/f.u.; the corresponding barrier for $BaZnF_4$ is 0.218 eV/f.u. For comparison, in the magnetic members of this fluoride family, with $M = Mn, Fe, Co$, and Ni , ΔE ranges from ~ 0.025 to ~ 0.2 eV/f.u.¹²; the conventional oxide perovskite ferroelectrics $BaTiO_3$ and $PbTiO_3$ have energy barriers of .018 and .200 eV/f.u. respectively³⁴.

Our calculated spontaneous polarizations, P_S , obtained from the difference in polarization between the undistorted $Cmcm$ PE phase and the $Cmc2_1$ FE ground state along the same branch of the polarization lattice are shown in Table II. We see that the values obtained using the Berry phase approach are similar to those obtained from multiplying the displacements of the ions with their formal ionic point charges (Ba^{2+} , M^{2+} , F^-), indicating that the Born effective charges, Z^* , are close to their formal values and that the ferroelectric mechanism is of geometric nature with no significant charge transfer between cations and anions¹². As stated above, we expect that these non-anomalous Born effective charges might lead to a different strain-polarization coupling from that found in conventional ferroelectrics and we investigate this next.

B. Effect of strain on the ferroelectric polarization

The thin film geometry, in which a \sim nm-thick layer of ferroelectric material is grown on a substrate or metallic electrode, is important in device architectures, and can be used to modify the ferroelectric behavior through

TABLE II. Spontaneous polarizations calculated by summing over the product of the formal charges times the displacements, using the Berry phase approach, and measured experimentally (\ddagger Ref. [11], \dagger Ref. [35], \star Ref. [36])

P_S (001)	BaMgF ₄ $\mu\text{C}/\text{cm}^2$	BaZnF ₄ $\mu\text{C}/\text{cm}^2$
Formal charges	8.9	11.4
Berry phase	10.1	13.2
Experimental	7.7 \ddagger	9.7 \ddagger
	6.9 \dagger	9.0 \star

strain induced via coherent heteroepitaxy with the substrate. In conventional perovskite ferroelectrics such strain-polarization coupling can be strong, leading for example, to the onset of ferroelectricity in otherwise paraelectric SrTiO₃³⁷ and the enhancement of the polarization and coercivity in ferroelectric BaTiO₃³⁸. First-principles studies¹⁷ have rationalized the magnitude of the strain dependence in terms of the material's piezoelectric and elastic constants, which in turn are often large in oxide ferroelectrics. Motivated by these features, and by the different nature of the ferroelectric polarization in the fluoride compounds, we now calculate the strain dependence of the ferroelectric polarization for BaMgF₄ and BaZnF₄.

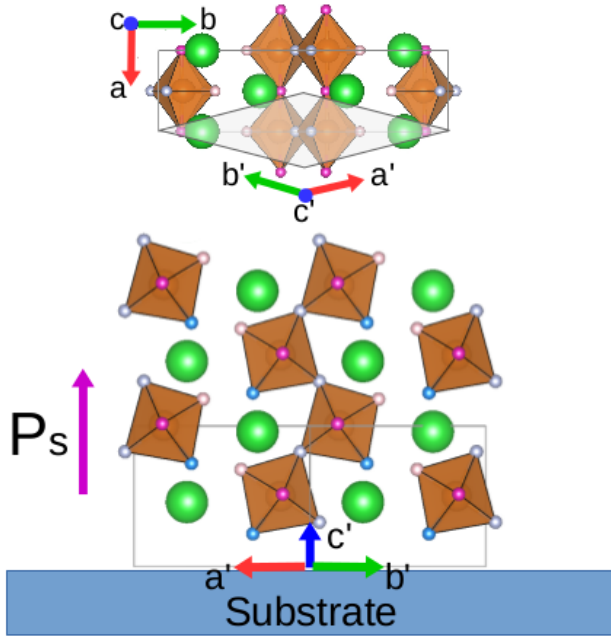


FIG. 4. Orientation of BaMF₄ relative to the substrate adopted in this work. The 12 atom primitive cell is indicated and compared to the 24 atom cell (top figure).

For our strain calculations, we use a 12-atom primitive cell, which is connected to the conventional unit cell through the relationships $\vec{a}' = \frac{1}{2}(a, -b, 2c)$, $\vec{b}' =$

$\frac{1}{2}(a, b, 2c)$ and $\vec{c}' = \vec{c}$, see Fig. 4. This choice of system of reference is convenient because in this set up $|\vec{a}'| = |\vec{b}'|$. Strain is generated by fixing the lattice parameters corresponding to the lateral directions of the substrate (a' and b'), relaxing the internal ionic degrees of freedom, and determining the out-of-plane lattice parameter (c') by means of an equation of state. We induce compressive and tensile strains between -3% and +3%, where the misfit strain is defined as $\epsilon = \frac{|\vec{a}'|}{|\vec{a}'_0|} - 1 = \frac{|\vec{b}'|}{|\vec{b}'_0|} - 1$. Note that in this orientation the ferroelectric polarization lies perpendicular to the plane of the film, a geometry that is desirable for device applications but in practice might be difficult to achieve through conventional layer-by-layer growth methods.

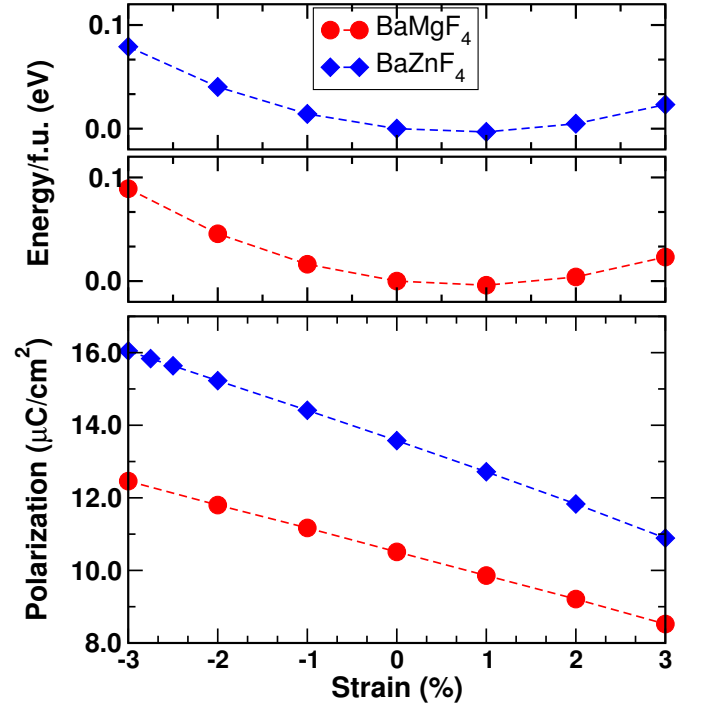


FIG. 5. (Color online) a) Energy per formula unit (f.u.) and b) spontaneous polarization P_S as a function of strain (ϵ) calculated using the Berry phase approach for BaMF₄ (M=Mg, Zn).

Our calculated internal energies and polarizations as a function of strain are shown in Fig. 5. The energy variations over the $\pm 3\%$ strain range are less than 0.3% for compressive strain and 0.1% for tensile strain with respect to the zero-strain energy (Fig. 5 a). Then, we note that the polarization direction remains along the out-of-plane crystallographic c -axis for all strain values studied, in contrast to many perovskite oxides in which the polarization becomes in plane for tensile strain. Indeed, the spontaneous polarization varies close to linearly with strain for the entire range considered, with variations in magnitude from around +20% to -15% for both compounds compared to their unstrained values. While less dramatic than in some oxide counterparts, these values

are not insignificant and should not be ignored in creating heterostructures with lattice-mismatched materials. This nearly linear response of the spontaneous polarization to strain, ϵ , indicates that the barium fluorides also satisfy the relationship discussed for conventional ferroelectrics in Ref. 17 that

$$\Delta P = \left(2c_{31} - \frac{c_{33}}{n}\right) \epsilon = c_{\text{eff}} \epsilon \quad (1)$$

Here ΔP is the change in polarization, c_{31} and c_{33} are components of the piezoelectric tensor, and n is the Poisson ratio. Our effective piezoelectric constants, c_{eff} , are $-65 \mu\text{C}/\text{cm}^2$ and $-86 \mu\text{C}/\text{cm}^2$ for BaMgF_4 and BaZnF_4 , respectively, comparable to that of rhombohedral $\text{BiFeO}_3(R3c)$ ($-85 \mu\text{C}/\text{cm}^2$) but an order of magnitude smaller than those of BaTiO_3 and PbTiO_3 . Our calculated electronic band structures (not shown) indicate minimal change in band gap with strain.

C. Ferroelectric Domains: Formation of 180° Domain Walls

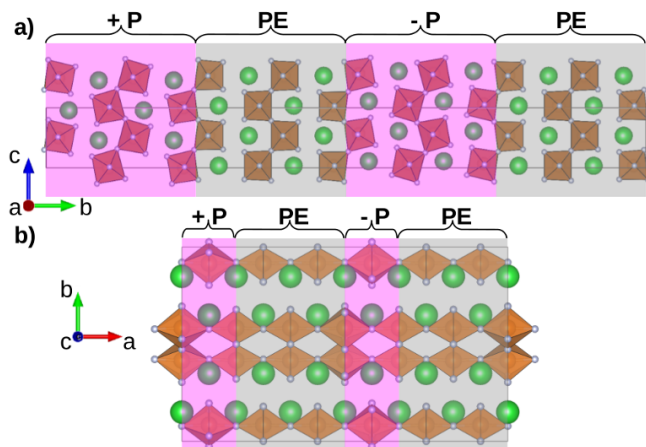


FIG. 6. Starting a) (101)-DW and b) (011)-DW configurations for BaMgF_4 (for BaZnF_4 the setup is analogous). We show two supercells along the c direction in a) only to help with visualization. Ions in PE regions (including the ones directly at the boundaries) are allowed to relax from the initial PE positions. The other regions have polarizations fixed along $+P$ and $-P$ respectively.

The domain walls between regions of differently oriented polarization in ferroelectrics are known to influence the ferroelectric switching behavior as well as to have functional properties in their own right^{39,40}. Much is known about the structure and energetics of domain walls in perovskite oxide ferroelectrics, both from first-principles density functional calculations (see for example Refs. [21, 41–44]) and from detailed experimental studies using for example high-resolution transmission electron microscopy (see for example Refs. [45] and [46]). However information about ferroelectric domain walls in the

BaMF_4 compounds is to our knowledge completely lacking; we provide the first calculations here.

In most domain walls, the component of polarization perpendicular to the wall is constant, so that

$$(\mathbf{P}_A - \mathbf{P}_B) \cdot \mathbf{n} = 0, \quad (2)$$

where \mathbf{P}_A and \mathbf{P}_B are the spontaneous polarizations of the two domains. This condition avoids a divergence of the electrostatic potential which would require a screening by additional charges and so such walls are called neutral (as opposed to charged) domain walls. In this work we restrict our discussion to neutral domain walls. In addition, we consider only 180° domain walls, in which the orientation of the polarization changes by 180° across the wall, and leave for other orientations such as 90° domain walls for future investigation. We explore two geometries, with the normal vector \mathbf{n} parallel to the crystallographic a - and b -axes in turn. To calculate the domain wall structures and energetics we construct supercells of the form $1 \times 4 \times 1$ times the primitive unit cell (containing 96 atoms) and $6 \times 1 \times 1$ times the primitive unit cell (144 atoms) for walls parallel to the ac - and bc -planes; we refer to these hereafter as (101)-DWs and (011)-DWs respectively. Within each supercell we impose two oppositely oriented domains with polarization parallel and antiparallel to the c axis and two domain walls. The central slabs of each domain are constrained to their calculated bulk ferroelectric structures (see Fig. 6). We then relax the atoms in the wall regions to their lowest energy configurations using the same convergence criteria as in Section II. The energy of a domain wall is then given by

$$E_{\text{domain wall}} = \frac{E - E_0}{2S}, \quad (3)$$

where E is the total energy of the supercell configuration in the presence of domain walls, E_0 is the reference energy of bulk BaMF_4 (computed for the same corresponding supercell), and S is the area of the domain wall (of which there are two per supercell). The convergence of the domain wall energies with respect to supercell size was tested by adopting different sizes with 72 and 96 atoms for the (101)-, and 96, 120, and 144 atoms for the (011)-DW configurations. The (011)-DWs converged more slowly and required larger supercells due to the corner sharing of the octahedra perpendicular to the domain wall. Table III shows our calculated energies for the two domain wall configurations investigated here as well as literature values for other selected ferroelectrics.

We see that the domain wall energies of the fluorides are similar to those of the oxides but we find no clear correlation between Curie temperature, magnitude of ferroelectric polarization, and domain wall energies for either the conventional ferroelectric perovskites or the geometric ferroelectric compounds.

We find that the domain wall energy is lowest for the (101)-DW configuration in BaMgF_4 and for the (011)-DW configuration in BaZnF_4 (although in the latter case the energies of the two wall types are very close). We

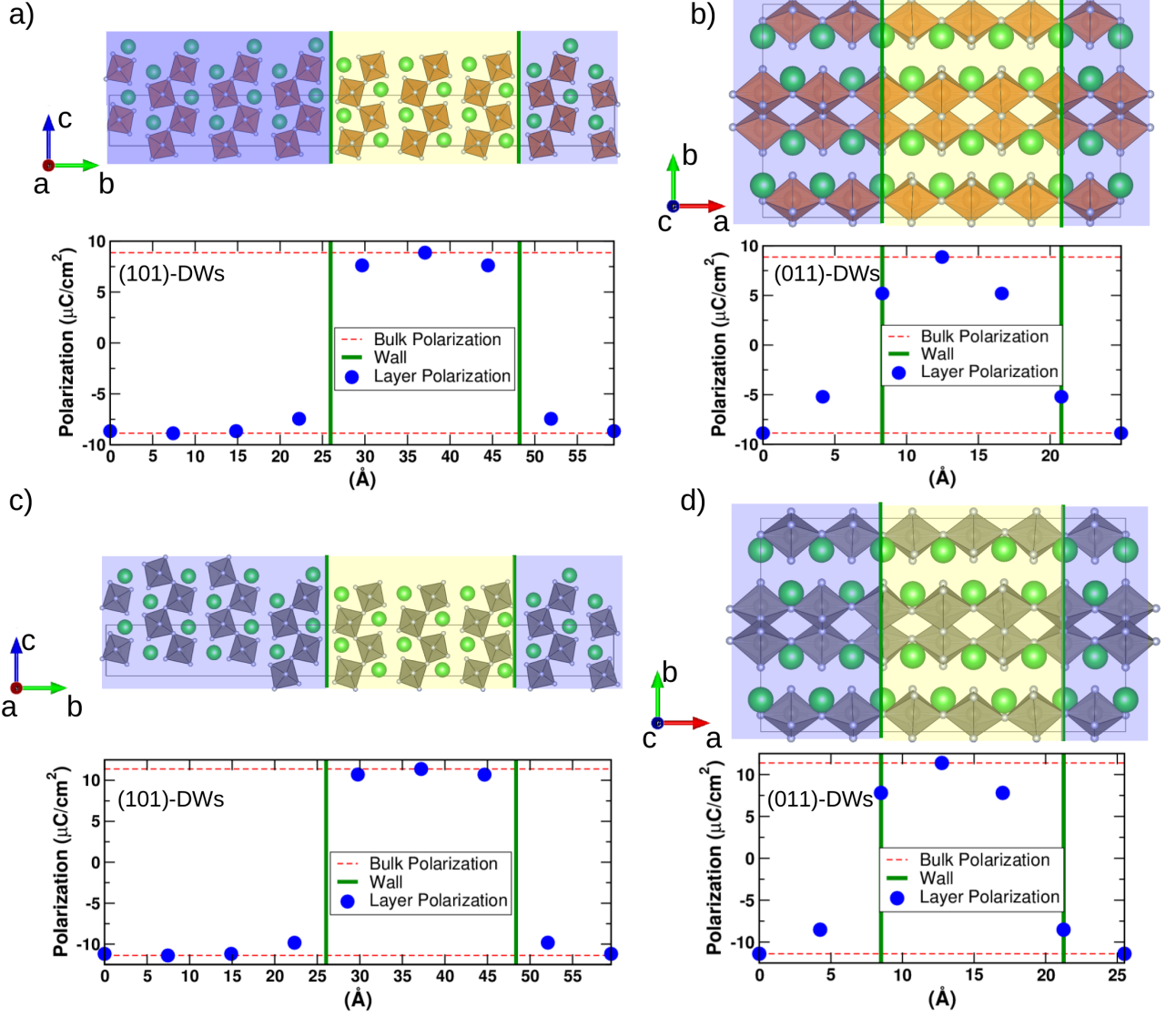


FIG. 7. (Color online) Layer Polarization in the (101)-DW and (011)-DW configurations for a,c) BaMgF₄ and b,d) BaZnF₄, respectively.

attribute this difference to the chemical activity of the Zn 3d electrons, although a detailed explanation is still lacking.

In Fig. 7 we show our calculated layer-by-layer polarizations perpendicular to the wall direction obtained from

$$P = \frac{e}{\Omega} \sum_{\alpha} Z_{\alpha} \cdot u_{\alpha}. \quad (4)$$

Here e is the charge of the electron, Ω the volume of a 1x1x1-cell layer, u_{α} is the displacement of atom α from its paraelectric position in the z -direction, Z_{α} are the formal ionic charges and the index α runs over all atoms in the considered 1x1x1-cell layer. Figs. 7a) and 7b) show our results for BaMgF₄ and Figs. 7c) and 7d) for

BaZnF₄. We find that the (101)-DW domain walls are sharp (Figs. 7a) and c)), that is, the local polarization changes abruptly across the domain wall from one bulk value to the opposite value. In contrast, our calculated lowest energy (011)-DW walls (Figs. 7b) and d)) show a smoother change in polarization across the wall. We can rationalize the difference in wall widths from the connectivity of the layers: While in the (101)-DW structures the wall lies between planes of MF₆ octahedra, in the (011)-DW the walls cut through the planes enforcing a gradual change of polarization across the wall. We note also that for both wall geometries, the MgF₆ octahedra retain their regular shape, but the ZnF₆ octahedra distort across the wall, particularly in the (011)-DW structure.

We point out that such atomically sharp domain walls

TABLE III. Domain wall energies calculated in this work for the (101)-DW (\dagger) and (011)-DW (\ddagger) configurations of BaMgF₄ and BaZnF₄, as well as the oxide ferroelectrics BiFeO₃, PbTiO₃ and hexagonal YMnO₃. The measured Curie temperatures and calculated polarizations are also shown for comparison. (References: \star -This work, \ast -[11], a -[47], b -[43 and 48], c -[49], d -[50], e -[51], f -[52], g -[42]).

Material	T_C (K)	P_S ($\mu\text{C}/\text{cm}^2$)	$E_{\text{domain wall}}$ (mJ/m^2)
BaMgF ₄	1263 \star	10.1	72 \dagger
			148 \ddagger
BaZnF ₄	1083 \star	13.2	185 \dagger
			159 \ddagger
BiFeO ₃	1103 a	90 a	80-800 b
PbTiO ₃	765 c	75 c	132 d
h-YMnO ₃	1258 e	5.6 f	11 g

are also observed in the improper ferroelectric hexagonal YMnO₃ series^{42,46} where they have been compared to the narrow twin planes formed at anti-phase boundaries in antiferrodistortive materials. Here the physics is similar, although the BaMF₄ series represents an unusual example of the behavior in a *proper* ferroelectric. In conventional ferroelectric perovskite oxides, while ferroelectric domain walls tend to be narrow, they are not atomically sharp.

IV. SUMMARY

In summary, using first-principles density functional theory we have calculated two properties of BaMgF₄ and

BaZnF₄ that are relevant for their behavior in ferroelectric thin films. First, we calculated the strain dependence of the spontaneous polarization and found that it varies close to linearly with both compressive and tensile strain indicating that it can be tuned in coherent thin-film heterostructures by appropriate choice of substrate lattice constant. Next, we calculated the energies and structures of neutral 180° domain walls and identified those most likely to occur in practical samples. We found that the domain wall energies are comparable to those of conventional oxide ferroelectrics, but that the wall thicknesses are thinner, reminiscent of twin boundaries in antiferrodistortive materials. We hope that our study motivates further experimental investigation of the BaMF₄ class of materials, and other unconventional ferroelectrics.

ACKNOWLEDGMENTS

This work was supported by ETH Zürich and by the ERC Advanced Grant program, No. 291151. Computations were performed at the Swiss Supercomputing Center and on the ETH Brutus cluster; final computational details and manuscript writing were completed at MIPT. The authors thank J. F. Scott for useful discussions.

-
- * nunez_valdez.m@mipt.ru
- ¹ O. Auciello, J. F. Scott, and R. Ramesh, Phys. Today **51**, 22 (1998).
 - ² P. Muralt, J. Micromech. Microeng. **10**, 136 (2000).
 - ³ Q. Zhang and R. W. Whatmore, J. Appl. Phys. **94**, 5228 (2003).
 - ⁴ B. W. Bessels, Annu. Rev. Mater. Res. **37**, 659 (2007).
 - ⁵ J. F. Scott, Rep. Prog. Phys. **12**, 1055 (1979).
 - ⁶ S. C. Buchter, T. Y. Fan, V. Liberman, J. J. Zayhowski, M. Rothschild, E. J. Mason, A. Gassanho, H. P. Jenssen, and J. H. Burnett, Opt. Lett. **26**, 1693 (2001).
 - ⁷ J. P. Meyn and M. Fejer, Opt. Lett. **22**, 1214 (1997).
 - ⁸ K. Momma and F. Izumi, J. Appl. Cryst. **41**, 653 (2008).
 - ⁹ H. G. v. Schnering and P. Bleckmann, Naturwiss. **55**, 342 (1968).
 - ¹⁰ M. Eibschütz, H. J. Guggenheim, S. H. Wemple, I. Camlibel, and M. D. Jr., Phys. Lett. **29A**, 409 (1969).
 - ¹¹ M. D. Jr., M. Eibschütz, H. J. Guggenheim, and I. Camlibel, Solid State Commun. **7**, 1119 (1969).
 - ¹² C. Ederer and N. A. Spaldin, Phys. Rev. B **74**, 024102 (2006).
 - ¹³ J. López-Pérez and J. Íñiguez, Phys. Rev. B **84**, 075121 (2011).
 - ¹⁴ F. Lichtenberg, A. Herrnberger, and K. Wiedemann, Prog. Sol. Stat. Chem. **36**, 253 (2008).
 - ¹⁵ B. B. van Aken, T. T. M. Palstra, A. Filippetti, and N. A. Spaldin, Nature Materials **3**, 164 (2004).
 - ¹⁶ C. J. Fennie and K. M. Rabe, Phys. Rev. B **72**, 100103(R) (2005).
 - ¹⁷ C. Ederer and N. A. Spaldin, Phys. Rev. Lett. **95**, 257601 (2005).
 - ¹⁸ S. Stemmer, S. K. Streiffer, F. Ernst, and M. Rühle, Philos. Mag. A **71**, 713 (1995).
 - ¹⁹ S. K. Streiffer, C. B. Parker, A. E. Romanov, M. J. Lefevre, L. Zhao, J. S. Speck, W. Pompe, C. M. Foster, and G. R. Bai, J. Appl. Phys. **83**, 2742 (1998).
 - ²⁰ J. Padilla, W. Zhong, and D. Vanderbilt, Phys. Rev. B **53**, R5969 (1996).
 - ²¹ B. Meyer and D. Vanderbilt, Phys. Rev. B **65**, 104111 (2002).
 - ²² C. Becher, L. Maurel, U. Aschauer, M. Lilienblum, C. Mag'en, D. Meier, E. Langenberg, M. Trassin, J. Blasco, I. P. Krug, P. A. Algarabel, N. A. Spaldin, J. A. Pardo, and M. Fiebig, Nature Nano. **10**, 661 (2015).
 - ²³ G. Kresse and J. Furthmüller, Phys. Rev. B **54**, 11169 (1996).

- ²⁴ P. E. Blöchl, Phys. Rev. B **50**, 17953 (1994).
- ²⁵ G. Kresse and D. Joubert, Phys. Rev. B **59**, 1758 (1999).
- ²⁶ P. Hohenberg and W. Kohn, Phys. Rev. B **136**, 864 (1964).
- ²⁷ W. Kohn and L. J. Sham, Phys. Rev. A **140**, 1133 (1964).
- ²⁸ J. P. Perdew, K. Burke, and M. Ernzerhof, Phys. Rev. Lett. **77**, 3865 (1996).
- ²⁹ R. D. King-Smith and D. Vanderbilt, Phys. Rev. B **47**, R1651 (1993).
- ³⁰ D. Vanderbilt and R. D. King-Smith, Phys. Rev. B **48**, 4442 (1994).
- ³¹ R. Resta, Rev. Mod. Phys. **66**, 899 (1994).
- ³² J. M. Posse, A. Grzechnik, and K. Friese, Acta Cryst. B **265**, 576 (2009).
- ³³ D. Cao, M. Q. Cai, C. H. Tang, P. Yu, W. Y. Hu, Y. Du, B. Y. Huang, and H. Q. Deng, Eur. Phys. J. B **74**, 447 (2010).
- ³⁴ R. E. Cohen, Nature **358**, 136 (1992).
- ³⁵ C. V. Kannan, K. Shimamura, H. R. Zeng, H. Kimura, E. G. Villora, and K. Kitamura, J. Appl. Phys. **104**, 114113 (2008).
- ³⁶ E. G. Villora, K. Shimamura, F. Jing, and A. Medvedev, Appl. Phys. Lett. **90**, 192909 (2007).
- ³⁷ J. H. Haeni, P. Irvin, W. Chang, R. Uecker, P. Reiche, Y. L. Li, S. Choudhury, W. Tian, M. E. Hawley, B. Craigo, A. K. Tagantsev, X. Q. Pan, S. K. Streiffer, L. Q. Chen, S. W. Kirchoefer, J. Levy, and D. G. Schlom, Nature **430**, 758 (2004).
- ³⁸ K. J. Choi, M. Biegalski, Y. L. Li, A. Sharan, J. Schubert, R. Uecker, P. Reiche, Y. B. Chen, X. Q. Pan, V. Gopalan, L.-Q. Chen, D. G. Schlom, and C. B. Eom, Science **306**, 1005 (2004).
- ³⁹ J. Seidel, L. W. Martin, Q. He, Q. Zhan, Y.-H. Chu, A. Rother, M. Hawkrige, P. Maksymovych, P. Yu, M. Gajek, N. Balke, S. V. Kalinin, S. Gemming, H. Lichte, F. Wang, G. Catalan, J. F. Scott, N. A. Spaldin, J. Orenstein, and R. Ramesh, Nature Materials **8**, 229 (2009).
- ⁴⁰ D. Meier, J. Seidel, A. Cano, K. Delaney, Y. Kumagai, M. Mostovoy, N. A. Spaldin, R. Ramesh, and M. Fiebig, Nature Materials **11**, 284 (2012).
- ⁴¹ A. Lubk, G. S., and N. A. Spaldin, Phys. Rev. B **80**, 104110 (2009).
- ⁴² Y. Kumagai and N. A. Spaldin, Nature Comm. **4**, 1540 (2013).
- ⁴³ O. Diéguez, P. Aguado-Puente, J. Junquera, and J. Íñiguez, Phys. Rev. B **87**, 024102 (2013).
- ⁴⁴ W. Ren, Y. Yang, O. Diéguez, J. Íñiguez, N. Choudhury, and L. Bellaiche, Phys. Rev. Lett. **110**, 187601 (2013).
- ⁴⁵ C. L. Jia, K. W. Urban, M. Alexe, D. Hesse, and I. Vrejoiu, Science **331**, 1420 (2011).
- ⁴⁶ Q. H. Zhang, L. J. Wang, X. K. Wei, R. C. Yu, L. Gu, A. Hirata, M. W. Chen, C. Q. Jin, Y. Yao, Y. G. Wang, and X. F. Duan, Phys. Rev. B **85**, 020102 (R) (2012).
- ⁴⁷ J. Wang, J. B. Neaton, H. Zheng, V. Nagarajan, S. B. Ogale, B. Liu, D. Viehland, V. Vaithyanathan, D. G. Schlom, U. V. Waghmare, N. A. Spaldin, K. M. Rabe, M. Wuttig, and R. Ramesh, Science **299**, 1719 (2003).
- ⁴⁸ A. Lubk, S. Gemming, and N. A. Spaldin, Phys. Rev. B **80**, 104110 (2009).
- ⁴⁹ B. Jaffe, W. R. Cook, and H. Jaffe, Acad. Press Inc. (1971).
- ⁵⁰ B. Meyer and D. Vanderbilt, Phys. Rev. B **65**, 104111 (2002).
- ⁵¹ A. S. Gibbs, K. S. Knight, and P. Lightfoot, Phys. Rev. B **83**, 094111 (2011).
- ⁵² N. Fujimura, T. Ishida, T. Yoshimura, and T. Ito, Appl. Phys. Lett. **69** (7), 1011 (1996).